# β-Sheet Pore-Forming Peptides Selected from a Rational Combinatorial Library: Mechanism of Pore Formation in Lipid Vesicles and Activity in Biological Membranes[†]

Joshua M. Rausch,[‡] Jessica R. Marks,[§] Ramesh Rathinakumar,[‡] and William C. Wimley*,[‡]

*Department of Biochemistry and Interdisciplinary Program in Molecular and Cellular Biosciences, Tulane University Health Sciences Center, New Orleans Louisiana 70112-2699*

ABSTRACT:  In a previous report we described the selection of potent, β-sheet pore-forming peptides from a combinatorial library designed to mimic membrane-spanning β-hairpins (Rausch, J. M., Marks, J. R., and Wimley, W. C. (2005) *Proc. Natl. Acad. Sci. U.S.A. 102*, 10511−10515). Here, we characterize their mechanism of action and compare the structure−function relationships in lipid vesicles to their activity in biological membranes. The pore-forming peptides bind to membrane interfaces and self-assemble into β-sheets that cause a transient burst of graded leakage across the bilayers. Despite the continued presence of the structured peptides in the bilayer, at most peptide concentrations leakage is incomplete and ceases quickly after peptide addition with a deactivation half-time of several minutes. Molecules up to 3,000 Da escape from the transient pores, but much larger molecules do not. Fluorescence spectroscopy and quenching showed that the peptides reside mainly on the bilayer surface and are partially exposed to water, rather than in a membrane-spanning state. The "carpet" or "sinking raft" model of peptide pore formation offers a viable explanation for our observations and suggests that the selected pore-formers function with a mechanism that is similar to the natural pore-forming antimicrobial peptides. We therefore also characterized the antimicrobial and cytotoxic activity of these peptides. All peptides studied, including non-pore-formers, had sterilizing antimicrobial activity against at least some microbes, and most have low activity against mammalian cell membranes. Thus, the structure−function relationships that were apparent in the vesicle systems are similar to, but do not correlate completely with, the activity of the same peptides in biological membranes. However, of the peptides tested, only the pore-formers selected in the high-throughput screen have potent, broad-spectrum sterilizing activity against Gram-positive and Gram-negative bacteria as well as against fungi, while having only small lytic effects on human cells.

A wide variety of pore-forming proteins and peptides take advantage of the discontinuous hydrophobicity of membrane-spanning β-sheets, which makes them well suited for undergoing transitions between hydrophilic and hydrophobic environments. For example, the β-barrel protein toxins including perfringolysin-O (*1*), α-hemolysin (*2*), and the anthrax protective antigen (*3*) preassemble a protein scaffold on membrane surfaces and then undergo a spontaneous transition in which loop sequences change conformation and are inserted into the membrane to form β-barrel pores. Similarly, there are many pore-forming, antimicrobial peptides (AMPs)[1] that are soluble in water and which self-assemble into β-sheet-rich pores in membranes (*4−6*). To explore the structural determinants of folding and self-assembly of β-sheets in synthetic and biological membranes we have been using rational combinatorial chemistry and high-throughput screening as learning tools to study peptides that spontaneously self-assemble into β-sheet pores in lipid vesicles (*7−9*). For the purpose of this work, we define a "pore" as any peptide-induced mechanism of membrane leakage without regard to structure or mechanism. The peptide library screened for pore-forming activity, shown in Figure 1, was designed to incorporate the common attributes of membrane-spanning β-hairpins into a 26 residue framework sequence. Combinatorial chemistry allowed a rapid top-down approach to determine which sequences favor pore-formation in lipid bilayer membranes over nonproductive processes such as aggregation.

Starting with an amphipathic dyad repeat framework (*10−12*) and six combinatorial sites within the membrane-spanning region we identified a single potent pore-forming motif from the 9,604 member library (*7*). With only six combinatorial sites in 26 residues there is a 77% identity among library members. The common framework consists
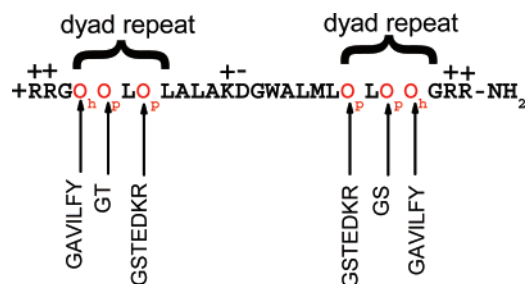
FIGURE 1: The rational combinatorial library used to select the peptides studied here. Details of library design, synthesis, and screening are given elsewhere (*7*). The library was designed to have a high propensity for membrane *β*-sheet formation by designing it to have two dyad repeats of alternating hydrophobic and hydrophilic amino acids (*10*, *11*). The KGDW sequence is consistent with a type I′ turn. The possible residues present in the combinatorially varied positions are shown as vertical columns. From this library of 9604 possible sequences 12 potent pore-formers were identified in vesicle-based high-throughput screens (*7*). These sequences are shown in Table 1.

Table 1: Peptide Sequences

| Peptide | Pore-forming Sequence[a] |
|---|---|
| FSSSTL | RRG**FS**L**S**LALAKDGWALML**SL**T**L**GRR |
| ➤ FSGRGY | RRG**FS**L**G**LALAKDGWALML**RL**G**Y**GRR |
| FSKGGY | RRG**FS**L**K**LALAKDGWALML**GL**G**Y**GRR |
| YGTKTF | RRG**YG**L**T**LALAKDGWALML**KL**T**F**GRR |
| YGKRGY | RRG**YG**L**K**LALAKDGWALML**RL**G**Y**GRR |
| ➤ FSSRGY | RRG**FS**L**S**LALAKDGWALML**RL**G**Y**GRR |
| YSRRTF | RRG**YS**L**R**LALAKDGWALML**RL**T**F**GRR |
| FSRKTY | RRG**FS**L**R**LALAKDGWALML**KL**T**Y**GRR |
| LSRRGF | RRG**LS**L**R**LALAKDGWALML**RL**G**F**GRR |
| ➤ YGKRGF | RRG**YG**L**K**LALAKDGWALML**RL**G**F**GRR |
| FSKRGF | RRG**FS**L**K**LALAKDGWALML**RL**G**F**GRR |
| FGRRTF | RRG**FG**L**R**LALAKDGWALML**RL**T**F**GRR |

| Negative Control Sequences | |
|---|---|
| ➤ AGGKGF[b] | RRG**AG**L**G**LALAKDGWALML**KL**G**F**GRR |
| GGEDGA[c] | RRG**GG**L**E**LALAKDGWALML**D**L**GA**GRR |

| Composite Positive Sequences[d] | |
|---|---|
| ➤ FSKRGY | RRG**FS**L**K**LALAKDGWALML**RL**G**Y**GRR |
| ➤ FGKRGY | RRG**FG**L**K**LALAKDGWALML**RL**G**Y**GRR |

*a* Sequences of the most potent pore-forming peptides selected from a 9604 member combinatorial library. Residues in bold/underline are positions that were varied in the library (Figure 1). *b* Negative control sequence from a well that had no visually detectible pore-forming activity at low stringency. *c* Designed negative peptide that has none of the six features of the pore-forming motif. This peptide does not form secondary structure and does not form pores in vesicles (unpublished observation). *d* Composite positive sequences that conform to the pore-forming motif, but were not actually observed in the library screen. Marked sequences were synthesized and purified for detailed characterization of pore-forming activity in this work.

of basic terminal residues, a pair of nine residue putative *β*-strand dyad repeats with hydrophobic external residues, and a potential type I′ turn (Figure 1). Internal alanine residues increase hydrophobicity to favor membrane partitioning (*13*). The variable residues include the intended membrane interface of both strands and four sites that are in register with the polar surface of the dyad repeat. In a stringent screen of 10,000 sequences, about a dozen very potent pore-forming peptides, assessed by the extent of leakage they caused in lipid vesicles, were identified (*7*). These peptides, which self-assembled into *β*-sheets in membranes, contained a consistent sequence motif that is similar to motifs found in naturally occurring pore-forming peptides: interfacial aromatic residues (*5*, *14*−*17*), a single interfacial hydroxyl group, and a basic residue within each presumed *β*-strand (*5*, *18*−*20*). Sequences are shown in Table 1.

Here we used biophysical methods to characterize the mechanism of leakage induced in lipid vesicles by these peptides. A variety of mechanisms have been proposed to describe the action of pore-forming peptides in membranes (*4*, *5*, *15*, *16*, *21*). These models range from molecular models of highly specific transmembrane pore structures like the one formed by gramicidin (*22*) to nonspecific colloidal models such as the so-called "carpet model" (*23*), "sinking raft model" (*24*), and their variants. In the vast literature on pore-forming peptides, convincing evidence for specific three-dimensional transmembrane pore structures is exceedingly rare. Nonetheless, the existence of a specific structure is assumed in many studies.

There are roughly 1000 known pore-forming peptides including toxins and antimicrobial peptides (*25*, *26*). Of those that have been studied carefully in lipid vesicles, most function by a mechanism that is not consistent with specific, stable transmembrane pore structure. For example most require a very high peptide concentration in the bilayer, amounting to hundreds or thousands of peptide molecules bound to each lipid vesicle. Furthermore, many pore-forming peptides induce partial leakage of vesicle contents through transient pores. Transient pores of this type typically form immediately after addition of peptide to bilayers causing partial leakage of contents, followed by rapid inactivation or closure of the pores by an unknown mechanism. Subse-

quent additions of peptide will result in a additional bursts of partial leakage.

In this work we address the mechanism of action of the pore-forming peptides that were selected from the rational combinatorial library shown in Figure 1 (*7*). We report evidence that these pore-formers, selected with no bias toward any particular mechanism of action, form pores by the "carpet model", a mechanism that is also observed for many of the natural pore-forming antimicrobial peptides. This mechanism is dependent on nonspecific self-assembly of peptides on membrane surfaces into peptide-rich domains that, in turn, drive destabilization of the bilayer and transient leakage of vesicle contents. The pore-forming peptides discovered by screening the *β*-hairpin library in lipid vesicles thus share features in common with naturally occurring, pore-forming antimicrobial peptides (AMP) (*27*). We hypothesized that the mechanism of pore-formation in biological membranes is also similar, however, the correlation between structure and function of pore-forming peptide in vesicles and in biological membranes remains controversial (*28*). Therefore, we characterized the antimicrobial and cytotoxic activity of four similar peptides originating from this framework that have very different structures and pore-forming propensities in vesicles, including members of the library that do not form pores in vesicles under stringent conditions. While the specific structure−function relation-

ships observed in lipid vesicles are not completely coupled to pore-forming activity in all microbial membranes, our data suggest a correlation between pore formation in vesicles and activity that is like natural AMPs, comprising *broad-spectrum* antimicrobial activity with little or no lytic activity against mammalian membranes. We discuss the implications of these observations for design and characterization of pore-forming and antimicrobial peptides.

## EXPERIMENTAL PROCEDURES

*Reagents.* Most chemicals and materials were purchased through Fischer Scientific (St. Louis, MO). Fluorescent dextrans, ANTS, DPX, DPA, and TbCl$_3$ were obtained from Molecular Probes (Eugene, OR). All lipids were obtained from Avanti Polar Lipids (Alabaster, AL). Fmoc-amino acids and other peptide synthesis reagents were purchased from Advanced Chemtech (Advanced Chemtech, Louisville, KY). Tryptophan octyl amide (TOA) was synthesized by coupling tryptophanamide to octanoic acid, followed by RP-HPLC purification. RPMI-1640, DMEM, fetal bovine serum, penicillin-streptomycin, and 3-(4,5-dimethylthiazol-2-yl)-2,5-diphenyltetrazolium bromide (MTT) were obtained from Sigma-Aldrich (St. Louis, MO). SYTOX green nucleic acid stain was obtained from Invitrogen (Carlsbad, CA).

*Peptide Synthesis.* Synthesis of peptides was carried out using 0.5 g (0.2 mmol/g) of Tentagel S-AM resin on an Applied Biosystems AP Pioneer peptide synthesizer (Applied Biosystems, Foster City, CA) using standard Fmoc strategies (*29*, *30*). Cleavage of peptide and removal of side-chain protecting groups was done by Reagent R (90% (v/v) trifluoroacetic acid, 5% thioanisole, 3% ethanedithiol, and 2% anisole) that was chilled on ice before adding it to the resin. The vessels were kept chilled for 30 min before removing to a bench top shaker for an additional 1.5 h. The trifluoroacetic acid solution was drained into silanized 20 mL glass vials, dried under nitrogen gas stream in a fume hood, washed multiple times with dichloromethane, and lyophilized multiple times from glacial acetic acid.

Lyophilized crude peptide was resuspended in DMSO and purified by reverse phase HPLC, using a Waters 600 HPLC pump system equipped with a Waters 486 in-line UV/vis absorbance detector (Waters Corporation, Milford, MA) and a Dynamax C18 fused silica column of dimensions 1 cm inner diameter and 30 cm length (Dynamax Inc., Houston, TX). Samples were eluted from the column using a gradient from 0 to 60% acetonitrile (0.1% TFA) and water (0.1% TFA) over 45 min. Fractions corresponding to the predominant peak were collected and dried. Identity of purified peptides was confirmed by MALDI mass spectroscopy at the LSU Protein Core Facility (Louisiana State University Health Sciences Center, New Orleans, LA) using a Perceptive Biosystems Voyager DE system (Applied Biosystems, Foster City, CA).

*Liposome Preparation.* Large unilamellar vesicles (LUV) of 100 nm diameter were prepared by extrusion (*31*, *32*) using lipids dried from chloroform and rehydrated with buffer. During the preparation of LUV, repeated freezing and thawing of lipid solutions was done to increase the encapsulation of reporter molecules. Dried lipid films were resuspended in buffer to a concentration of 100 mM lipid to maximize encapsulation. For LUV encapsulating Tb$^{3+}$, a resuspension buffer of 50 mM TbCl$_3$, 100 mM sodium citrate, and 10 mM TES, pH 7.2, was used. Tb$^{3+}$ LUV were diluted to 25 mM lipid for the extrusion process, due to increased viscosity. ANTS/DPX LUV were prepared with a resuspension buffer of 10 mM potassium phosphate, pH 7.0, 25 mM ANTS, and 5 mM DPX. Dextran containing LUV used a buffer of 10 mM potassium phosphate, pH 7.0, 10 mg/mL labeled dextran. To ensure maximal encapsulation, 20 cycles of freeze thaw were used in preparation of dextran LUV. Following extrusion, LUV samples were run over a gel filtration column (4 cm i.d., 40 cm length) of Sephadex G-200 equilibrated to elution buffer. In the case of dextran encapsulation, unlabeled dextrans were added to the buffer at 10 mg/mL to eliminate osmotic pressure on the vesicles.

*Leakage Assays.* Assays to assess the extent of dye leakage from liposomes were performed at 500 $\mu$M lipid concentrations, and peptide concentrations were varied between 1 and 10 $\mu$M, or 1:50 through 1:500 peptide to lipid (P:L) ratio. Peptides were mixed with lipid solutions by inversion of the cuvette five times followed by 2 h incubation for peptides to have full effect. Fluorescence was recorded using excitation and emission wavelengths of 270 and 490 nm, for Tb$^{3+}$/DPA fluorescence and 350 and 510 nm for ANTS/DPX. Fluorescence corresponding to complete release was determined by Triton X-100 solubilization of the vesicles.

Fluorescent dextrans were entrapped in LUV at concentrations of 10 mg/mL, sufficient to obtain measurable self-quenching. External labeled dextran was exchanged with unlabeled dextran using gel filtration chromatography. Peptides were added to 500 $\mu$M lipid solution in 10 mM potassium phosphate, pH 7, at P:L ratios of 1:50 and 1:500 and mixed by inversion of cuvette five times. After 15 min, fluorescence of samples was recorded using 8 nm bandwidths on an SML Aminco 8100 spectrofluorometer. For the 3 kDa dextran labeled with rhodamine, excitation and emission wavelengths were 545 and 600 nm, respectively. For the 40 kDa dextran labeled with fluorescein, excitation and emission wavelengths were 465 and 530 nm, respectively. Leakage was measured by relief of self-quenching. Fluorescence corresponding to complete release was determined by Triton X-100 solubilization of the vesicles.

*ANTS/DPX Requenching Assay.* The requenching assay was used to determine mechanism of leakage as described previously (*6*, *33*, *34*). Briefly, peptides were added from a stock solution to 2.5 mL of assay solution in a quartz cuvette with a rotating stir bar. Assay solution consists of 500 $\mu$M lipid vesicles with entrapped ANTS and DPX in 10 mM potassium phosphate, pH 7. To a series of individual samples, increasing concentration of peptide was added and the leakage was allowed to proceed for 2 h, until complete. Then, the quencher DPX was titrated in externally to quench the ANTS that had leaked out. ANTS that remains entrapped is not quenched by externally added DPX. Finally, an excess Triton X-100 was added to assess the fluorescence intensity for complete leakage. Calculation of the fraction of ANTS released and the quenching of the ANTS that remained entrapped within vesicles was done as we have previously described (*6*, *33*, *34*).

*Peptide Partitioning.* Peptide partitioning into lipid bilayers was determined spectroscopically by fluorescence methods described by White et al. (*35*, *36*). Partitioning of peptides into lipid bilayers was monitored by the fluorescence

enhancement of tryptophan upon addition of lipid vesicles. Fluorescence was recorded using excitation wavelength of 270 nm and scanning for emission between 290 and 500 nm with 8 nm bandwidths. Measurements were carried out in 10 mM potassium phosphate, pH 7. Peptides were added from DMSO stock solutions or from 0.1% acetic acid stock to 500 $\mu$L of buffer and mixed by inversion.

Fluorescence scans were analyzed using Origin 5.0 software (Origin Lab Corp., Northampton, MA). Scans were subtracted for background and lipid scattering effects and compensated for scattering loss by scaling to free tryptophan samples at the same lipid concentration (*36*). From these data, the area under the curve was taken as a measure of the intensity (*I*) of tryptophan fluorescence. Intensity values were normalized to peptide in buffer ($I_0$). Mole fraction partition coefficients ($K_x$) were obtained by fitting the formula

$$\frac{I}{I_0} = 1 + (I_{\max} - 1)\left(\frac{K_x[\mathrm{L}]}{K_X[\mathrm{L}] + [\mathrm{W}]}\right)$$

where *I* is the fluorescence intensity, $I_0$ and $I_{\max}$ are the intensities before lipid addition and after saturation of binding, [L] is the lipid concentration, [W] is the molar concentration of water (55.3 M), and $K_x$ is the mole fraction partition coefficient. Measured partition coefficients were independent of peptide concentration, indicating "infinite dilution" conditions such that we are measuring a true partition coefficient. However we note that that the contribution of electrostatic interactions is influenced by experimental details such as bilayer surface charge and ionic strength (*37*, *38*), and these partition coefficients are thus specific for our experimental conditions.

*Tryptophan Quenching.* The effects of the collisional quencher iodide ($\mathrm{I}^-$) were used to probe the exposure of the Trp residue at position 15 of the peptides (Figure 1). Peptides were added to 10 mM potassium phosphate buffer, pH 7, and scanned followed by a titration with KI. A second series of samples were prepared with 1 mM lipid. Quenching of the Trp was similar in the two experiments with Stern−Volmer quenching constants greater than 4 $\mathrm{M}^{-1}$ for all peptides, indicating significant water exposure of the Trp residue of bound peptides. For comparison free tryptophan has a quenching constant of around 8 $\mathrm{M}^{-1}$.

For doxyl-PSPC quenching experiments, LUV were prepared either with lipid compositions of 90% POPC and 10% POPG or with 87.5% POPC + 2.5% of 5-, 10-, or 16-doxyl-PSPC lipids plus 10% POPG. Peptides were added to 10 mM phosphate buffer pH 7 to a concentration of 1 $\mu$M. Fluorescence emission scans were collected before and after the addition of 1 mM lipid. The effects of doxyl-PSPC were determined by comparison to standard 90% POPC, 10% POPG LUV.

*Circular Dichroism.* Peptides were dissolved in 0.025% acetic acid solution with brief vortexing and sonication in a Fisher FS 60 bath sonicator. Concentrations were measured by UV absorbance at 280 nm. The peptides were diluted into 10 mM potassium phosphate, pH 7, and spectra were recorded on a Jasco 810 spectropolarimeter (Jasco Inc., Easton, MD) between 190 and 280 nm using a quartz cuvette with 0.1 cm path length. Spectra were taken before and after the addition of 2 mM LUV composed of 90% POPC and 10% POPG. Spectra are corrected for small background lipid

and buffer contributions and represented as mean molar ellipticity ($\Theta$).

*Membrane Fusion.* Experiments to detect membrane fusion during leakage were performed with a fluorescence resonance energy transfer (FRET) technique using NBD and rhodamine-labeled lipids (*39*). In brief, the fluorescence of the donor (NBD) is quenched by the presence of the acceptor (rhodamine) in a concentration dependent manner. Fusion of labeled and unlabeled vesicles dilutes the dye concentrations in the bilayer and relieves the quenching. In the FRET fusion assays we used 25 $\mu$M vesicles composed of 19:1 POPC:POPG LUV with NBD-POPE and rhodamine-POPE (Avanti Polar Lipids, Alabaster, AL) concentrations of 2.5% and 1% mol fraction of total lipid, respectively. NBD is the fluorescent donor, and rhodamine is the acceptor. A 19-fold excess of unlabeled POPC:POPG LUV was then added to the system to a total lipid concentration of 500 $\mu$M. The fluorescence spectra for these samples were recorded from 480 to 750 nm on an SLM Aminco 8100 spectrofluorometer with excitation at 465 nm in a 4 mL quartz cuvette containing a stir bar. An initial spectrum was obtained for 2.5 mL of this solution before a time trace was performed to monitor NBD emission at 530 nm. Detergents or peptides in DMSO were added to sample after 1 min. Fusion was measured at 1:50 and 1:100 P:L ratios where it was observed. No fusion occurred at P:L ratios higher than 1:100. Triton X-100 was added after the time course to samples and the emission spectrum measured again for normalization.

Control vesicles were prepared as separate LUV solutions representing serial 2 fold dilutions of dye concentrations within bilayers. Control LUV were prepared at NBD/rhodamine POPE concentrations of 1.25%/0.5%, 0.63%/0.25%, 0.31%/0.13% and 0.16%/0.06% as well as LUV with only 2.5% NBD-POPE or 1% rhodamine-POPE. These LUV are representative of 1, 3, 7, 15, and an infinite number of fusion events assuming that all vesicles undergo uniform fusion with unlabeled LUV. Stocks of each of these labeled LUV solutions were prepared with unlabeled LUV to 500 $\mu$M in proportions such that the overall concentration of lipid and dye is maintained. The NBD fluorescence at 530 nm can then be used to calculate the extent of membrane fusion observed upon addition of peptide to the standard assay solution with NBD-POPE and rhodamine-POPE concentrations of 2.5% and 1%. Using the curve obtained for LUV standards, the amount of fusion occurring upon peptide addition is calculated from an empirical relationship that correlates fluorescence with the number of fusion events. The inclusion of LUV individually labeled with NBD- or rhodamine-POPE represented a theoretical absolute fusion whereby the dyes are in separate bilayers. Using this empirical curve we quantitate fusion in unknown samples quantitated by the number of theoretical fusion events that have taken place.

*Antimicrobial Activity.* Microbes (*Escherichia coli* NapIV, *Pseudomonas aeruginosa* PA01, *Staphylococcus aureus* FDA 209, and *Cryptococcus neoformans* 184-A) were grown to midlogarithmic phase and diluted to $10^4$ colony forming units (CFU)/mL with liquid test medium (10% growth broth in PBS). 120 $\mu$L of cells were incubated with serial dilutions of selected peptides for 3 h at 37 °C, 180 $\mu$L assay. 125 $\mu$L of 2× concentrated growth medium was added to the cell solution, and cells were allowed to recover overnight, ~18

h. Visual inspection and optical density at 600 nm was used to evaluate cell growth. Typically, wells were either opaque (OD > 0.5), indicating stationary phase growth, or they were transparent (OD < 0.02), indicating no growth. Aliquots from wells with no apparent growth were spread on nutrient agar plates to verify sterility. In all cases there were <100 CFU/mL in those wells compared to $10^7$ CFU/mL in the opaque wells. In many cases transparent wells contained zero CFU. The lowest concentration of peptide that prevented cell growth is the minimum sterilizing concentration (MSC). All MSC measurements are the average of 3−8 independent experiments.

*Hemolytic Activity.* To determine if the $\beta$-sheet pore-formers could also permeabilize a robust eukaryotic membrane we tested hemolysis in sheep and human erythrocytes. A 10% (v/v) suspension of erythrocytes (Lampire Biological Laboratories, Pipersville, PA) was incubated with different concentrations of selected peptides (*40*). Cells were diluted to $7.7 \times 10^6$ cell/ mL and incubated at room temperature for 1 h with peptide (0.5 $\mu$M, 5$\mu$M, or 15 $\mu$M). The samples were then centrifuged at 10000$g$ for 5 min, and the heme absorbance in the supernatant was measured at 410 nm. Baseline was defined by RBC incubated with PBS only and lysis was normalized to 15 $\mu$M melittin, a peptide concentration that causes complete lysis and by osmotic lysis with distilled water.

*Cytotoxicity against Living Mammalian Cells.* MV4:11 leukemia cells/HEK293T cells ($5 \times 10^5$ cells/mL) grown in RPMI-1640/DMEM + 10% FBS and 1% penicillin-streptomycin were treated with 5$\mu$M of peptide or an equivalent volume of buffer (positive control). Following addition of peptides, the cell suspension was incubated for 72 h at 37 °C with 5% $CO_2$ in a humidified incubator. 50 $\mu$g of 3-(4,5-dimethylthiazol-2-yl)-2,5-diphenyltetrazolium bromide (MTT) (Sigma) was added, and then cells were incubated for 6 h. Formazan crystals were then dissolved using acidified isopropanol (90% isopropanol:10% Triton-X-100: 0.4% HCl), and the optical density at 550 nm was measured using a plate spectrophotometer. Fractional MTT activity was obtained by comparing peptide treated samples to cells treated with buffer only and wells with no cells.

*Permeabilization of Microbial Membranes. E. coli* was grown in TSB at 37 °C to reach its late exponential growth phase (OD$_{600}$ ~0.5), and then cells were centrifuged, washed, and suspended in PBS for membrane permeability experiments. Cell suspension in PBS ($2 \times 10^7$ cells/mL) was incubated with 1 $\mu$M SYTOX green for 15 min in the dark. Then 5 $\mu$M of peptides was added to the cell suspension, and the increase in fluorescence was measured (excitation wavelength at 485 nm and emission at 520 nm) immediately over a time scale of 0 to 30 min. SYTOX green is not membrane permeable. Its fluorescence increases only when the bacterial inner membranes are permeabilized and the dye can interact with the cellular DNA.

## RESULTS

*Peptide Membrane Interactions.* The fluorescence enhancement of tryptophan was used to determine mole fraction partition coefficients in the method described by White et al. (*35*). Upon titration with vesicles composed of 90% POPC and 10% POPG fluorescence of the tryptophan residue at
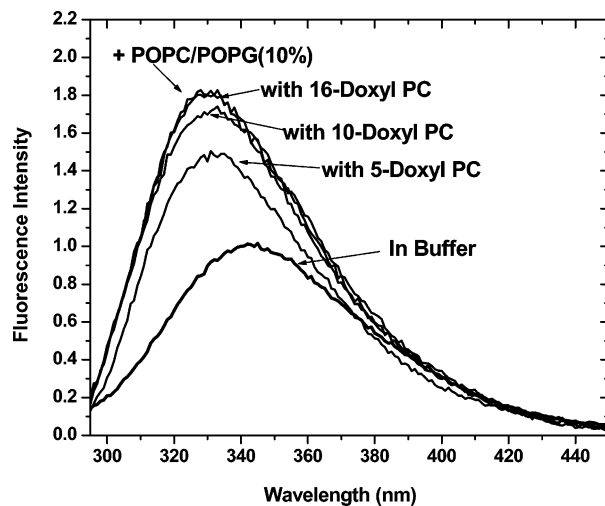


FIGURE 2:  Binding and quenching of tryptophan in pore-forming $\beta$-sheet peptides. Fluorescence emission spectra are shown for peptide FSKRGY in buffer at about 10 $\mu$M, and after addition of 1 mM lipid vesicles made from 90% POPC and 10% POPG which produces a large blue shift of the emission maximum, and after addition of vesicles which also contained 1 mol % of doxyl-labeled PC lipids. These quenching experiments are used to determine the depth of penetration of the tryptophan residue and indicate an interfacial location rather than a transmembrane one.
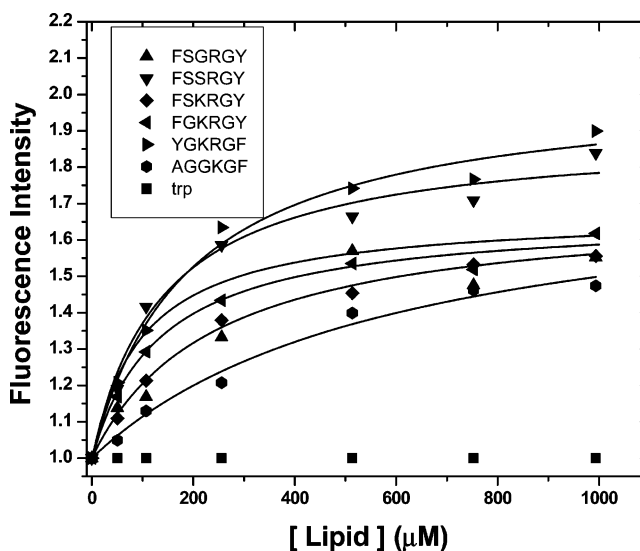


FIGURE 3:  Fluorescence titration of tryptophan fluorescence at 330 nm with increasing amounts of lipid vesicles. Peptide binding to large unilamellar vesicles made from 90% POPC and 10% POPG produces an increase in fluorescence intensity indicative of binding. Binding was measured by tryptophan fluorescence titration using about 10 $\mu$M peptide and monitoring the intensity of tryptophan fluorescence. Mole fraction partition coefficients were calculated from the binding isotherms as described elsewhere (*35*). All peptides studied bind to membranes with similar partition coefficients.

position 15 increased by an average of 1.7-fold (Figures 2 and 3). The wavelength of maximum emission shifted from 350 nm in buffer to about 330 nm when bound to lipid vesicles (Figure 2). Mole fraction partition coefficients ($K_x$) ranged from 1 to $4 \times 10^5$ (Table 2). For any experiment the fraction of peptide bound can be calculated by fraction bound = $K_x[L]/(K_x[L] + 55)$, where $K_x$ is the apparent mole fraction partition coefficient, [L] is the lipid concentration (molar), and 55 is the molar concentration of water. This is an infinite dilution measurement in which partition coefficients are independent of peptide concentration. However because there

Table 2: Peptide Interactions with Bilayers

| peptide | $K_x$ $(\times 10^5)^a$ | fluorescence enhancement[b] | $\lambda_{max}$ in vesicles (nm)[c] | 5-doxyl PSPC[d] | 10-doxyl PSPC | 16-doxyl PSPC[e] | quench by KI[f] |
|---|---|---|---|---|---|---|---|
| FSGRGY | 2.9 | 1.68 | 331 | 0.80 | 0.93 | 0.93 | ++ |
| FSSRGY | 3.7 | 1.90 | 331 | 0.86 | 0.93 | 0.93 | ++ |
| FSKRGY | 2.3 | 1.70 | 330 | 0.86 | 0.98 | 1.00 | ++ |
| FGKRGY | 3.9 | 1.67 | 330 | 0.86 | 1.00 | 1.00 | ++ |
| YGKRGF | 2.9 | 2.01 | 329 | 0.88 | 0.94 | 1.00 | ++ |
| AGGKGF | 1.0 | 1.80 | 332 | 0.85 | 0.92 | 0.94 | ++ |
| melittin | 16.3 | 1.55 | 321 | 0.75 | 0.83 | 0.92 | + |
| TOA | 5.4 | 1.55 | 339 | 0.87 | 0.80 | 0.87 | − |

[a] Mole fraction partition coefficient calculated from fluorescence titration experiment (Figure 2). [b] Enhancement is the ratio of the tryptophan fluorescence intensity at 330 nm in lipid vesicles to the intensity in buffer. Lipid vesicles are composed of 90% POPC/10% POPG. [c] The wavelength of maximum emission after interaction with lipid vesicles. $\lambda_{max}$ in buffer is between 344 and 350 nm. [d] Doxyl spin labeled lipids quench Trp fluorescence in a distance dependent manner. The doxyl-labeled lipids we use here are labeled near the lipid−water interface (5-doxyl), midway along the acyl chains (10-doxyl), or at the midplane of the hydrocarbon core of the bilayer (16-doxyl). Quenching is defined as intensity in the presence of 1% doxyl lipids divided by the intensity without doxyl lipids. [e] Unlike the 5- and 10-doxyl labels, the 16-doxyl labels from both monolayers are at approximately the same depth in the bilayer, leading to an effective concentration of 16-doxyl lipid at the bilayer midplane that is twice the local concentration of the 5- and 10-doxyl labels. Thus quenching by 16-doxyl lipids is exaggerated. [f] Quenching by KI is a measure of water exposure of the Trp residue. All peptide tryptophans were quenched by KI at least 50% as well as free tryptophan (++), indicating significant water exposure.

are electrostatic interactions, the values are dependent on experimental conditions such as ionic strength (*41*). All of the peptides studied here have similar membrane binding. In fact, most members of the library bind membranes well (unpublished observation), which is not surprising when the compositional similarity of the library members is considered. Importantly, this means that the differences in pore-forming potency that we are exploring are not due to differences in membrane binding, but rather to differences in self-assembly and membrane disruption that occurs after the peptide is bound.

*The Location of the Peptides in the Bilayer.* The wavelength of maximum emission of the tryptophan of these pore-forming peptides in lipid bilayers was around 330 nm, suggesting an interfacial location of the Trp residue at position 15 (*36*). The location of the peptides with respect to the bilayer plane was further investigated using fluorescence quenching techniques. Experiments were done using doxyl labeled lipids as membrane-bound, depth dependent quenchers (*5, 6*). The doxyl group was anchored at different depths of the lipid bilayer through attachment to the 5, 10, or 16 carbon of a stearoyl (C18:0) chain of a PC lipid. Tryptophan fluorescence spectra were collected for peptides in buffer and when mixed with 1 mM lipid (Figure 2). The fluorescence enhancement of tryptophan was determined. Comparison of enhancement between vesicles containing different spin labeled lipids showed that the 5-doxyl PSPC had the greatest quenching effect on the peptides, including AGGKGF. Several peptides were not quenched at all by the 16-doxyl lipids. Taken together, the $\lambda_{max}$ of Trp fluorescence and the doxyl quenching results indicate a interfacial location of the tryptophan residue at position 15. Similarly, an aqueous quencher of tryptophan, potassium iodide (KI), was used to assess the aqueous phase exposure of the tryptophan residues of the peptides and accessibility to buffer. The library-derived peptides all had significant KI quenching that was comparable to that of free tryptophan (Table 2). This is also consistent with the tryptophan residue being localized to the interfacial region of the lipid bilayer where it is exposed to lipids and water simultaneously.

The same quenching experiments were performed on two standards, tryptophan octyl amide (TOA) and the helical

pore-forming peptide melittin. TOA is a simple tryptophan analogue known to partition strongly into membranes and bury itself in the hydrocarbon chains of the bilayer (*42*). For TOA the most pronounced quenching occurred with the 10-doxyl PSPC. KI had no effect on TOA fluorescence once it was fully partitioned into bilayers. The bee venom, pore-forming peptide melittin has a unique tryptophan at position 19. This residue was quenched equally well by 5- and 10-doxyl PSPC, indicating that the melittin tryptophan has penetrated deeper into the bilayer than the library-derived peptides. Melittin was less affected by KI in experiments than library-derived peptides, indicating that it was less exposed to the buffer.

*Secondary Structure.* Circular dichroism (CD) was used to characterize the secondary structure of the peptides that had been designed to favor β-hairpin formation (Figure 1). In buffer, the pore-forming peptides had CD spectra with a small negative band at 218 nm, indicative of a partial β-sheet structure (*43*). Upon addition of the peptide to 1 mM lipid, the β-sheet content increases (Figure 4) for most of the peptides as observed in the wavelength shift for the negative band to around 215 nm and increased ellipticity at 195 nm. The CD spectra in lipid are consistent with ordered β-sheets (*44*). The selected non-pore-forming control peptide, AGGKGF, exhibited a CD spectrum characteristic of a random coil in buffer that changed to a α-helix upon titration with lipid. The designed negative GGEDGA was unstructured in buffer and had a small amount of helical content in lipid bilayers (Figure 4).

*Peptide Induced Leakage from Vesicles.* The purified peptides were assayed for their ability to induce $Tb^{3+}$/DPA and ANTS/DPX leakage from vesicles. The peptides were assayed at various peptide to lipid (P:L) ratios. Vesicles composed of 90% POPC and 10% POPG were used in most experiments, but we also performed some experiments using pure POPC and bilayers containing 10% POPG and up to 30% cholesterol. In semiquantitative plate-based screens (*9*) similar pore-forming activity was observed for all lipid compositions studied. All selected pore-forming peptides are active against all lipid compositions down to 1:500 P:L, the conditions of the high-throughput screen. AGGKGF did not induce leakage in these assays.
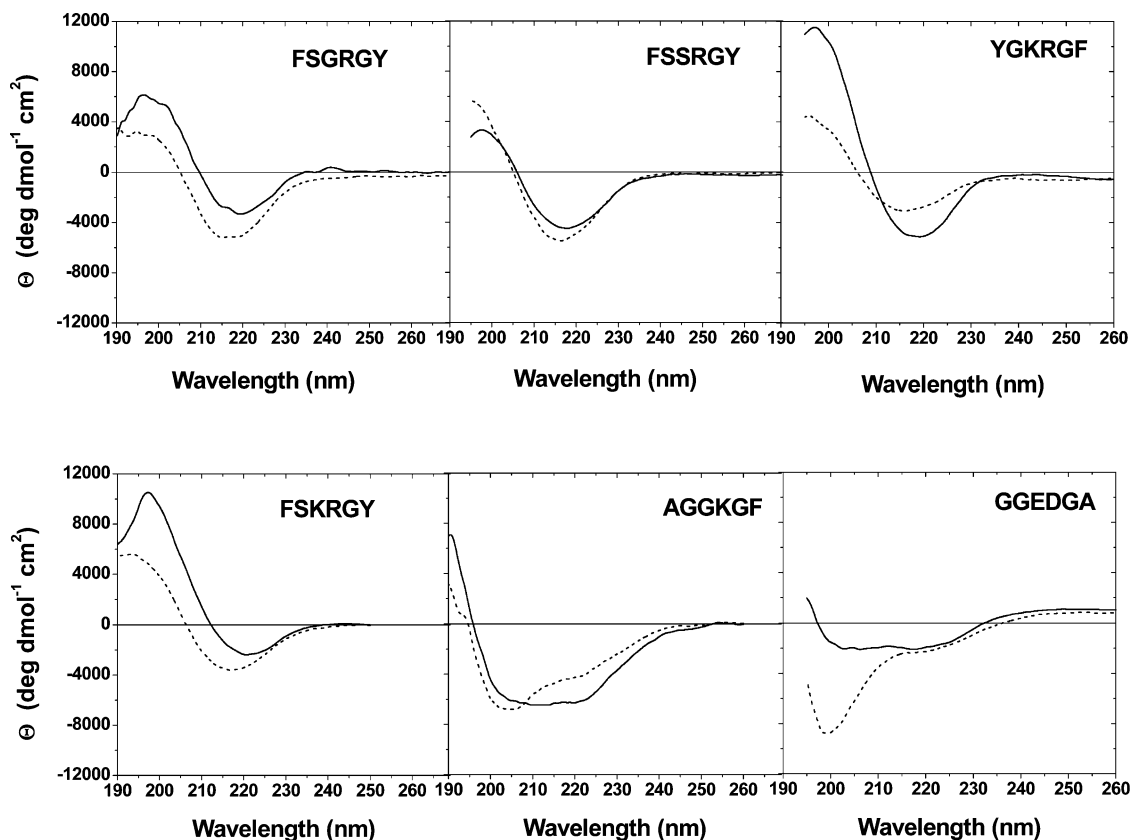
FIGURE 4: Circular dichroism spectroscopy. For circular dichroism spectroscopy, peptides were added to 50 mM potassium phosphate buffer (pH 7) or to phosphate buffer containing 2 mM large unilamellar vesicles made from 90% POPC and 10% POPG. Peptides were added from stock solutions of 1−5 mM in dilute acetic acid up to a concentration of roughly 50 $\mu$M. Actual concentrations were determined by UV absorbance. Multiple scans at 10 nm/min scan rate were averaged, and a similarly collected background was subtracted. Dotted lines are for the peptides in buffer and solid lines are for the same concentration of peptide in the presence of 2 mM lipid vesicles. All pore-forming peptides had some $\beta$-sheet content in buffer which increased in lipid vesicles.

Time dependence of $Tb^{3+}$ and ANTS fluorescence was similar and showed that leakage was a rapid and transient process, with most leakage occurring within the first minutes after peptide addition (Figure 5). Within 15 min of peptide addition leakage from vesicles had stopped. This is despite the fact that the vesicles still contained entrapped markers and despite the fact that the peptides were still bound to the membranes with $\beta$-sheet secondary structure. This enigmatic observation of transient pore formation, which is difficult to explain using models of particular transmembrane peptide structures, has been made in many other peptide pore-formers also.

*The Size of the Pores Formed in Bilayers.* Molecules of different size were used to estimate the size of the transient pores formed by the peptides. Large pores or detergent-like solubilization of the bilayer will produce leakage without solute size dependence (*45*) while pores smaller than about 20 Å will show size dependence of permeability (*6, 45*). All peptides were tested for their ability to induce leakage of lipid encapsulated fluorescent indicators of different molecular weights. The $Tb^{3+}$ assay employs components of about 150 g/mol, which are oppositely charged and separated by the membrane. The ANTS/DPX assay uses probes of about 425 g/mol each having charged moieties and diameters of 5 to 8 Å. We also used fluorescent-labeled dextrans of either 3,000 or 40,000 g/mol average molecular weight. Dextrans have an ellipsoidal shape, with a short axis of ∼20 Å diameter but differing in their long axis. The effective
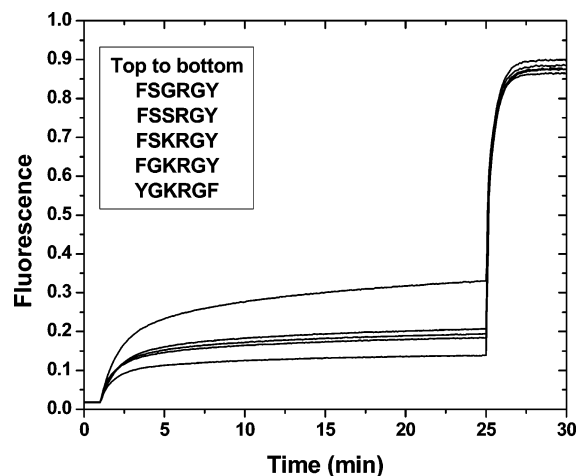


FIGURE 5: Leakage of $Tb^{3+}$ from large unilamellar vesicles induced by the pore-forming peptides selected in high-throughput screens. In all experiments, 1 $\mu$M peptide was added from a stock solution in 0.1% acetic acid to a cuvette containing 100 $\mu$M lipid vesicles with entrapped $Tb^{3+}$ and external DPA. Peptide: lipid ratio is thus 1:100. Leakage of $Tb^{3+}$ from the vesicles increases fluorescence (*34*) due to interaction with the external chelator DPA. The peptides induce a burst of leakage that is nearly stopped by 10 min. At 25 min, Triton X-100 was added to completely disrupt the vesicles and release 100% of the contents.

hydrodynamic radii of 3 kDa and 40 kDa dextrans have been reported to be 18 and 25 Å (*46*) respectively. The question of whether larger dextrans can reptate through peptide pores

Table 3: Leakage Assayed with the Terbium/DPA Assay and the ANTS/DPX Assay

| peptide | 1:50 P:L | 1:100 P:L | 1:250 P:L | 1:500 P:L |
|---|---|---|---|---|
| | | Tb/DPA Leakage[a] | | |
| FSGRGY | 37% | 26% | 11% | 7% |
| FSSRGY | 33% | 28% | 13% | 7% |
| FSKRGY | 33% | 28% | 13% | 9% |
| FGKRGY | 27% | 26% | 12% | 7% |
| YGKRGF | 31% | 22% | 11% | 6% |
| AGGKGF | 4% | <1% | <1% | <1% |
| melittin | 100% | 100% | 100% | 54% |
| alamethicin | 100% | 100% | 100% | 100% |
| | | ANTS/DPX Leakage[a] | | |
| FSGRGY | 100% | 86% | 47% | 28% |
| FSSRGY | 73% | 63% | 46% | 30% |
| FSKRGY | 85% | 77% | 38% | 24% |
| FGKRGY | 100% | 84% | 45% | 25% |
| YGKRGF | 100% | 72% | 42% | 33% |
| AGGKGF | <1% | <1% | <1% | <1% |
| melittin | 100% | 100% | 86% | 36% |
| alamethicin | 100% | 100% | 100% | 100% |

[a] Leakage was measured by mixing lipid vesicles with entrapped dyes and monitoring fluorescence intensity. See text for details. After about 15 min leakage had usually stopped. Intensity was measured after several hours of incubation. The intensity for 100% leakage was determined after the addition of Triton X-100 to completely solubilize the bilayers.

Table 4: Peptide-Induced Leakage of Dextrans from Vesicles

| | dextran leakage | | | |
|---|---|---|---|---|
| | 3 kDa dextran[a] | | 40 kDa dextran[b] | |
| peptide | 1:50 P:L | 1:500 P:L | 1:50 P:L | 1:500 P:L |
| FSGRGY | 60% | 32% | 12% | 7% |
| FSSRGY | 65% | 26% | 8% | 4% |
| FSKRGY | 78% | 43% | 15% | 6% |
| FGKRGY | 83% | 41% | 13% | 6% |
| YGKRGF | 65% | 21% | 18% | 12% |
| AGGKGF | 9% | 5% | 8% | 5% |
| melittin | 43% | 7% | 12% | 12% |
| alamethicin | 39% | 12% | 13% | 6% |

[a] Rhodamine-labeled dextran of 3000 Da molecular weight was entrapped within vesicles at 10 mg/mL. [b] Fluorescein-labeled dextran of 40,000 Da molecular weight was entrapped in lipid vesicles at 10 mg/mL. Leakage of dextran is monitored by fluorescence because release from vesicles relieves self-quenching and increases intensity. Fluorescence intensity for complete release is determined after solubilizing the vesicles with the detergent Triton X-100.

has not been resolved, but the clear distinction between 3 and 40 kDa molecules is a reasonable measure of apparent "pore" size.

As shown in Tables 3 and 4, the selected pore-forming peptides induced measurable, concentration-dependent leakage of $Tb^{3+}$/DPA, ANTS/DPX, and the 3 kDa dextran at concentrations as low as 1:500, a P:L ratio consistent with the high-throughput selection conditions (7). It is interesting to note that the ANTS/DPX assay always reports higher leakage than the Tb/DPA assay, despite using larger probes. This is probably because terbium(III) exists in solution as a citrate chelated complex (47) having an effective diameter of around 10 Å and a higher charge density. Very little leakage of the 40 kDa dextran was observed under any conditions. AGGKGF did not induce significant leakage in any of these assays. These experiments show that the pore-forming peptides selected from the library can only release molecules that are roughly 20 Å in diameter or smaller,

consistent with reports of other pore-forming antimicrobial peptides (6). The control peptides are the toxins alamethicin and melittin that partition into bilayers and may assemble into membrane-spanning barrel-stave or toroidal pores made from the association of 4 to 8 helices (48). These two peptides caused complete leakage of $Tb^{3+}$/DPA and ANTS/DPX under nearly all conditions tested. As expected from the hypothetical pore structure of melittin and alamethicin, neither allowed leakage of the larger dextran. However, some leakage of the 3 kDa dextran was observed for melittin and alamethicin at the 1:50 P:L conditions. These results demonstrated a significantly smaller pore for melittin and alamethicin compared to that observed for the library peptides.

*Mechanism of Leakage.* Partial leakage of vesicles contents through transient pores is a common mechanism of action of antimicrobial peptides. Transient, partial leakage can occur in one of two modes. Leakage can be a graded process, whereby all vesicles leak a portion of their contents, or an all-or-none process, where a fraction of the vesicles release all of their contents while the rest retain their contents completely (6, 33). All-or-none leakage occurs when pore formation is a rare stochastic process, such that only a fraction of the vesicles have had a pore self-assemble in their membrane. Graded leakage occurs when all vesicles experience an equal probability of transient, low-conductance pore formation during which some fraction of the vesicle contents are released. It has been demonstrated previously that the mechanism of leakage can be determined experimentally using the ANTS/DPX system followed by "requenching," or titration of the system with exogenous DPX, after the peptide-induced leakage had stopped (33, 34). The ANTS/DPX requenching method was used to determine the mechanism of leakage for the library-derived peptides in order to differentiate the possible mechanism of pore formation.

The general theory of the requenching method (6) is as follows. After the initial burst of peptide-induced leakage has occurred (Figure 6) some ANTS remains entrapped within the vesicles and some has been released. The solution is then titrated with external DPX to quench the external ANTS. This allows determination of the extent to which ANTS molecules still retained within the vesicles are quenched. Two values are obtained in such an experiment: $f_{out}$, the fraction of ANTS released, and $Q_{in}$, the degree of quenching of the ANTS that is still entrapped within the vesicles. The value for $f_{out}$ is varied by conducting independent experiments at increasing P:L ratios. In all-or-none leakage, the ANTS in the vesicles which failed to leak their contents would still be subject to the original level of internal quenching ($Q_{in}$), thus $Q_{in}$ versus $f_{out}$ is a horizontal line. If leakage is by a graded leakage mechanism, both the ANTS and DPX will be partially released from all vesicles to some extent during fractional leakage, thereby decreasing the local concentration of DPX inside the vesicles. This decreases the quenching inside the vesicles ($Q_{in}$ increases toward 1.0). Both mechanisms have been observed (6, 33). The results of the requenching experiments are presented in Figure 6. The results are similar for all the β-sheet pore-formers, which are plotted together. The value of $Q_{in}$ increases dramatically as $f_{out}$ increases. Thus, the transient, peptide induced leakage (Figure 5) is occurring by a graded mechanism in which all of the vesicles leak a portion of their contents during the burst of leakage that follows addition of peptide. The
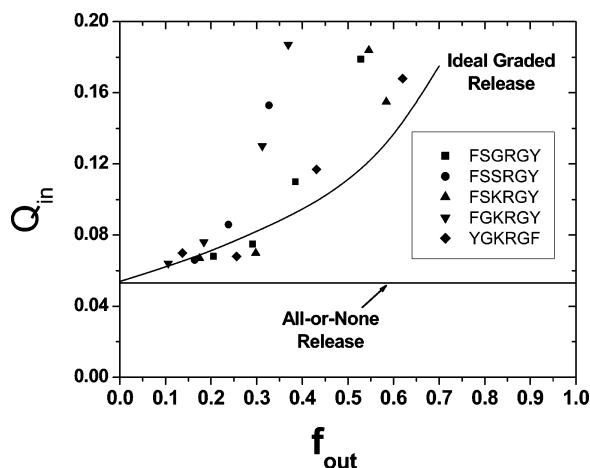
FIGURE 6: Mechanism of leakage assessed by the requenching method. The requenching method, described in detail elsewhere (*33*), can be used to distinguish graded release, in which all vesicles release a portion of their contents, from all-or-none release, in which a fraction of the vesicles release all of their contents. In a requenching measurement, peptide is added to vesicles containing ANTS and DPX and the leakage is allowed to occur (see Figure 5). After leakage has stopped the quencher DPX is titrated into the cuvettes and fluorescence is measured again. In this way the fraction of ANTS released and the quenching of the entrapped contents ($Q_{in}$) can be determined. If release is graded, then $Q_{in}$ will increase with $f_{out}$ because the concentration of DPX decreases inside the vesicles. On the other hand, if release is all or none, then $Q_{in}$ will remain unchanged because those vesicles that did not release their contents will have the same initial concentration of entrapped DPX. These two possible outcomes are drawn in the plot. Release caused by the pore-forming peptides follows a graded release mechanism in which all vesicles release a portion of their contents during the burst of leakage that follows peptide addition.

observation that $Q_{in}$ increases slightly faster than for ideal graded leakage indicates that DPX leaks from vesicles slightly faster than ANTS, a phenomenon we have previously observed (*34*).

*Effects of Peptides on Bilayer Stability.* The classical image of peptide pore formation involves a specific, membrane-spanning, three-dimensional structure, while other models evoke images of peptide-rich domains in which the bilayer integrity is compromised. To assess the overall destabilization of bilayer integrity by our pore-forming peptides, we measured membrane fusion of large unilamellar vesicles caused by the pore-forming peptides using Förster resonance energy transfer (FRET) (*39*). Local destabilization of bilayer integrity should result in fusion of the bilayers as well as leakage. To assess fusion, LUV were prepared with of NBD- and rhodamine-labeled lipids. At 1 mol % of the FRET acceptor rhodamine, near total quenching of the NBD is attained. Labeled LUV were then mixed with a 19-fold excess of unlabeled 9:1 POPC:POPG LUV, up to 500 $\mu$M total lipid concentration. Fusion between labeled and unlabeled vesicles decreases the concentration of the FRET acceptor rhodamine and increases NBD fluorescence (Figure 7). In the absence of peptide, these vesicles were very stable over time and no fusion occurred. Addition of the pore-forming peptides at P:L = 1:50 to 90:10 POPC/POPG caused a small increase in NBD fluorescence, indicating that some fusion is occurring. The number of fusion "events" that would account for the observed increase in NBD fluorescence is between 3 and 6 (see Experimental Procedures above) for the pore-formers. AGGKGF caused much less fusion than
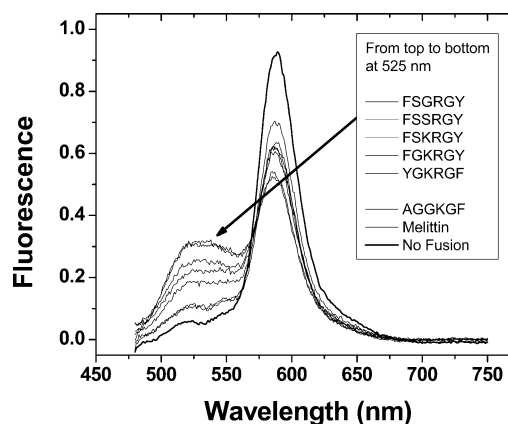


FIGURE 7: Membrane fusion induced by the pore-forming $\beta$-sheet peptides. Membrane fusion was measured with a fluorescence resonance energy transfer (FRET) technique using NBD and rhodamine-labeled lipids (*39*). In brief, the fluorescence of the donor (NBD) at 520 nm is quenched by the presence of the acceptor (rhodamine) in a concentration dependent manner. Fusion of labeled and unlabeled vesicles dilutes the dye concentrations in the bilayer and relieves the quenching causing an increase in donor fluorescence at 520 and a decrease in acceptor fluourescence at 580 nm. We used 25 $\mu$M vesicles composed of 19:1 POPC:POPG LUV with NBD-POPE and rhodamine-POPE at 2.5 and 1 mol % fraction of total lipid, respectively. A 19-fold excess of unlabeled POPC:POPG LUV was then added to the system to a total lipid concentration of 500 $\mu$M. Curves shown are for P:L = 1:50 of the indicated peptides. Using the curve obtained for vesicle standards, the amount of fusion occurring upon peptide addition can be calculated as described in the text. The pore-forming peptides caused a moderate amount of fusion at P:L 1:50, but not at higher P:L.

the pore-formers (number of events < 2) at P:L 1:50. For assays at 1:250 or 1:500 P:L conditions we observed little or no fusion with any peptide (not shown). Alamethicin and melittin have been well studied for their barrel-stave or toroidal pores, and neither is known to cause severe distortion of bilayer integrity at low peptide concentration. In this assay, we observed little fusion in this system (number of fusion events ≤ 1.0) at any concentration of melittin or alamethicin tested. These results suggest that the $\beta$-sheet pore-formers do, in fact, destabilize bilayers consistent with our proposed mechanism for self-assembly and leakage. Importantly, the absence of fusion at peptide concentrations that cause leakage (Table 3 and 4) demonstrates that fusion is not required for leakage.

*Peptide $\beta$-Framework Is Sufficient for Bactericidal Activity.* Based on studies with *Staph. aureus*, we reported that a pore-forming peptide from the library had better antimicrobial activity than a non-pore-former (*7*). For this work, we studied additional peptides and tested the peptides against the Gram-negative bacteria *E. coli* and *P. aeruginosa* and against the fungus *Cryptococcus neoformans*, in addition to the Gram-negative bacteria *Staph. aureus*. We show here that the correlation between function in lipid vesicles and biological membranes is not as simple as first reported. Peptides were assessed for bactericidal activity based on the ability of the peptide to sterilize a culture of $10^4$/mL of *E. coli*, *P. aeruginosa*, or *S. aureus* at peptide concentrations of 15 $\mu$M or less (Figure 8). Cells were incubated with serially diluted peptide for 3 h in minimal media. A nutrient rich media was added, and the cells were subsequently allowed to recover overnight. A plate reader was used to measure opacity. Sterilized wells were as transparent as
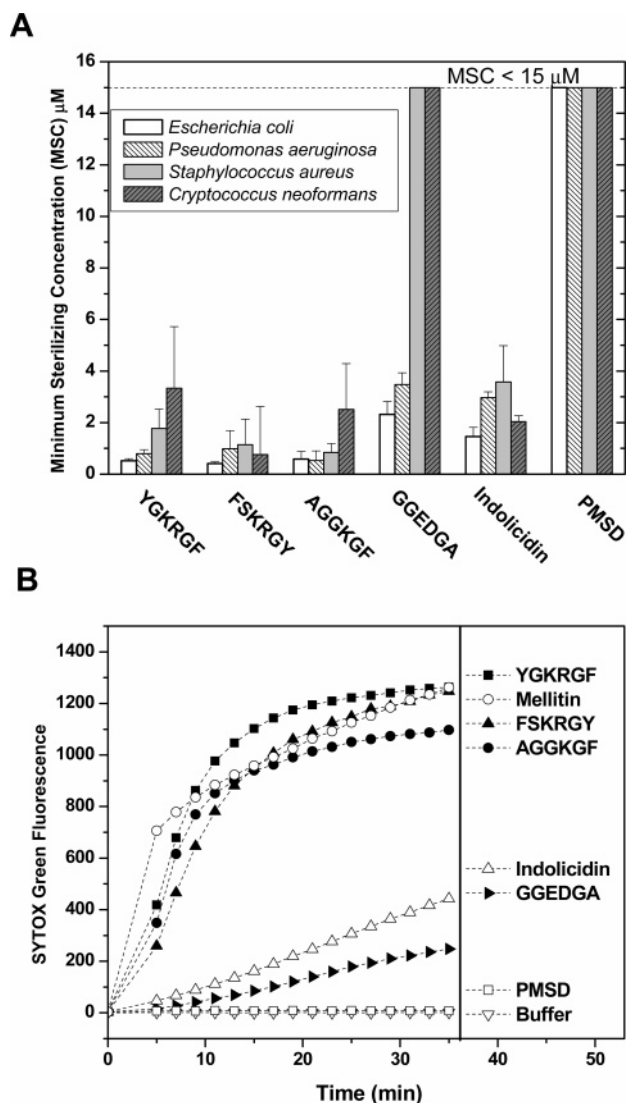
FIGURE 8: Antimicrobial activity of the peptides. A: Minimum sterilizing concentration (MSC) was measured by performing a serial dilution assay with a 15 $\mu$M starting peptide concentration. Microorganisms were grown to midlogarithmic phase and diluted to $10^5$ colony forming units (CFU)/mL with liquid test medium, 5% growth broth in PBS. 120 $\mu$L of cells was incubated with serial dilutions of selected peptides for 3 h at 37 °C, 180 $\mu$L assay. 125 $\mu$L of 2× concentrated growth broth was added to the cell solution, and cells were allowed to recover overnight, ~18 h. Optical density at 600 nm was used to evaluate cell growth. Typically, wells were either opaque (OD ~ 0.5), indicating stationary phase growth or they were transparent (OD < 0.02), indicating no growth. Wells with intermediate optical densities were rare. Aliquots from wells with no apparent growth were spread on nutrient agar plates to verify sterility. In all cases there were <100 CFU/mL in those wells compared to $10^7$ CFU/mL in the opaque wells. The average lowest concentration of peptide that prevented cell growth (OD peptide well = OD of buffer only well) is given as the minimum sterilizing concentration (MSC). Each measurement is the average of about 5 individual experiments. Means and SEM were calculated using dilution number and then converted to concentration. B: SYTOX Green/DNA binding dye assay for membrane permeabilization. In these experiments $10^7$ *E. coli* cells were equilibrated in 96 well plates in buffer containing the membrane-impermeable, DNA binding dye SYTOX Green. At time zero, 5 $\mu$M peptide or buffer only was added and the fluorescence caused by DNA binding of the SYTOX Green dye was monitored. Melittin is used as a control peptide because it caused maximal SYTOX Green binding at 5 $\mu$M peptide or above due to membrane lysis. All of the antimicrobial peptides caused immediate SYTOX green permeation across the bacterial membranes.

buffer (OD < 0.02), while nonsterilized wells grew to log phase and were turbid (OD > 0.5). Very few wells had optical densities between these two extremes. All of the library-derived peptides sterilized at least some of the bacteria species tested at low $\mu$M concentrations (Figure 8A). The $\beta$-sheet pore-formers YGKRGF, FSKRGY, and the $\alpha$-helical non-pore-former AGGKGF sterilize all of the bacterial cultures at concentrations of ~2 $\mu$M. The designed non-pore-former GGEDGA is less effective, sterilizing the two Gram-negative bacteria at concentrations ~4 $\mu$M but not killing *S. aureus*, a Gram-positive bacterium at concentrations up to 15 $\mu$M. All peptides share the same 20 residue framework of two potential dyad repeat segments connected by a four-residue turn, suggesting that this framework is sufficient for some bactericidal activity. In initial surveys of the antimicrobial activity of other peptides conforming to the pore-forming motif (*7*) we found that all have potent antimicrobial activity against *E. coli*. It is interesting to note that FSKRGY, YGKRGF, and AGGKGF have sterilizing antimicrobial activity at concentrations roughly 2-fold lower than the natural antimicrobial peptide indolicidin (Figure 8A).

We also used the SYTOX Green DNA binding dye (Figure 8B) to verify that the antimicrobial activity is correlated with permeabilization of the microbial membranes. In all cases, the broadly antimicrobial peptides rapidly permeabilize microbial membranes. The rate and extent of membrane permeabilization was similar to that caused by the lytic toxin melittin. Interestingly, the designed negative peptide, GGEDGA, which has the most limited spectrum of antimicrobial activity, is also the least effective at permeabilizing *E. coli* membranes. However it permeabilized *E. coli* membranes about as well as indolicidin and has sterilizing antimicrobial activity against this organism at this concentration.

*Antimicrobial Assessment of Controls.* The negative control peptide, the perfringolysin O membrane-spanning domain (PMSD), adopts a membrane-spanning $\beta$-hairpin conformation in the context of the membrane-bound protein multimer (*1*, *49*). Like the framework of the peptides of this study, PMSD contains dyad repeat sequences of potential amphipathic $\beta$-sheets. However, unlike the peptides designed in our lab, PMSD does not wholly conform to the common characteristics of AMPs. PMSD is anionic, with a net charge of −2. The hydrophobic-to-charged residue ratio is 3:1, outside the 1:1 to 2:1 range typical for AMPs, and the amino acids that are common in AMP sequences make up less than half of the peptide. Accordingly, PMSD is unable to induce leakage (unpublished observation) in vesicles and completely lacks antibacterial activity, suggesting that amphipathic $\beta$-hairpin propensity is not sufficient for bactericidal activity and supporting our framework as a unique AMP template. The positive control peptide indolicidin, a defensin isolated from bovine neutrophils (*50*), has sterilizing antimicrobial activity in the range of 2−4 $\mu$M as reported previously (*14*, *50*).

*The Pore-Forming Motif Also Correlates to Antifungal Activity.* To test whether the pore-forming peptides have the broad spectrum activity typical of natural antimicrobial peptides, we also tested the ability of the peptides to sterilize a liquid culture of the fungus C*ryptococcus neoformans*. All three of the peptides with at least one aspect of the pore-forming motif, FSKRGY, YGKRGF, and AGGKGF, sterilized fungal cultures within a narrow concentration range of

$4.5 \pm 0.9$ $\mu$M (Figure 8). However, GGEGDA, with none of the pore-forming motif features in the combinatorial sites, was unable to kill *C. neoformans* at any concentration. PMSD had no effect on *Cryptococcus*, and indolicidin sterilized the fungus at around 2 $\mu$M peptide.

*Peptides Do Not Have Broad Membrane-Lytic Activity.* Finally, we conducted experiments with sheep and human erythrocytes as well as living human cell lines to determine if these peptides were broadly membrane-lytic, like the bee venom toxin melittin, or were selectively toxic to microbes like most natural antimicrobial peptides. First we tested the ability of the peptides to lyse sheep erythrocytes, which are bounded by a very robust plasma membrane, as well as human erythrocytes. A characteristic of natural antimicrobial peptides (*4*, *16*) is that they do not readily lyse mammalian cells whereas potent membrane-lytic toxin peptides will lyse any membrane, including the robust ruminant erythrocyte membranes. Peptides were incubated with erythrocytes in PBS. Hemolysis was determined optically by measuring hemoglobin released compared to a buffer-only control. Melittin, the lytic peptide positive control, completely lysed the cells at a concentration of 5 $\mu$M peptide (Figure 9A). Hemolysis caused by the library-derived peptides was much lower. The peptides AGGKGF, YGKRGF, and indolicidin caused a moderate amount of concentration-dependent lysis, significant only at the highest peptide concentration studied (15 $\mu$M). None of the $\beta$-hairpin framework peptides caused substantial lysis at antimicrobial concentrations, therefore the library derived pore-forming peptides are not broadly membrane-lytic pore-formers. Interestingly, AGGKGF, which is a helical non-pore-former in vesicles, caused little lysis of sheep erythrocytes, but did cause significant lysis of human erythrocytes at the highest concentration studied.

Similarly, neither the pore-formers nor the control peptides PMSD and indolicidin have significant cytotoxic activity against living human cell lines (Figure 9B). The pore-forming peptides, like natural antibiotic peptides, are much more active against microbial membranes than mammalian membranes. The only exception is the peptide AGGKGF, which was toxic to MV4:11 cells, just as it was also hemolytic in human erythrocytes, at 15 $\mu$M peptide. As expected, melittin was highly toxic toward all mammalian cells.

## DISCUSSION

*Mechanism of Membrane Leakage.* A complex image of peptide-induced leakage in lipid vesicles emerges from these experiments. At a typical P:L ratio of 1:100, about 1000 peptides with $\beta$-sheet secondary structure bind rapidly to each vesicle and begin to cause almost immediate leakage of the vesicle contents. Molecules as large as 3 kDa, with hydrodynamic radii as large as 18 Å, leak from the bilayers. Despite the fact that the peptides remain bound to the vesicles and do not change secondary structure, the rate of leakage slows hyperbolically with a half-time of a few minutes and approaches zero within about 15 min. Thus the "pores" are transient, rather than equilibrium structures that form immediately following peptide binding, and are rapidly inactivated or dissipated by an unknown process.

To determine the mechanism of leakage observed it is imperative to explore the physical requirements for leakage from lipid vesicles. A large unilamellar vesicle has a diameter
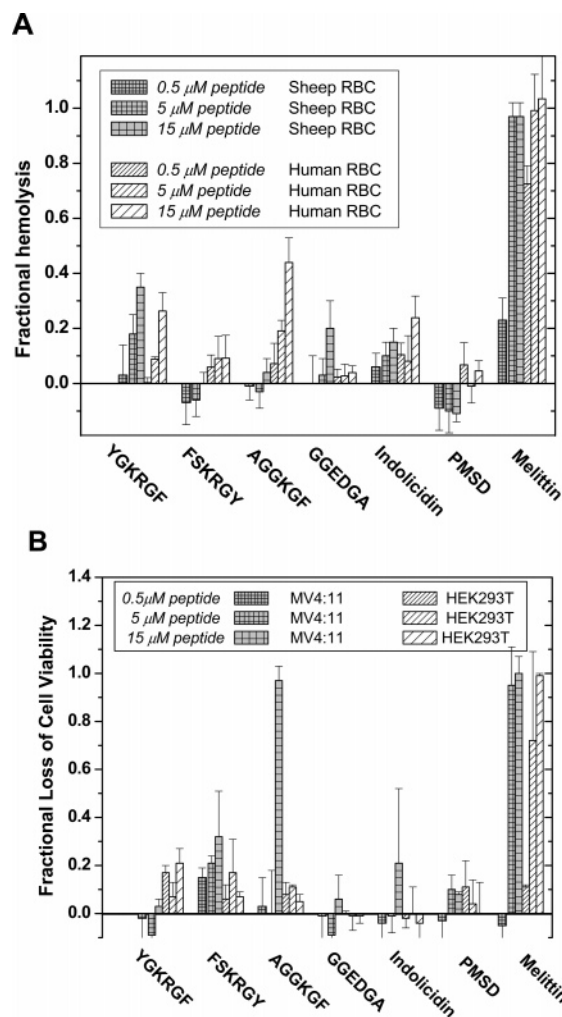


FIGURE 9:  Activity against mammalian cell membranes. A: Hemolytic activity of the pore-forming and antimicrobial peptides. 10% (v/v) suspensions of sheep or human erythrocytes were incubated with different concentrations of selected peptides (*40*). Red blood cells (RBC) were diluted to $7.7 \times 10^6$ cell/ mL and incubated at room temperature for 1 h with 0.5 $\mu$M, 5$\mu$M, or 15 $\mu$M peptide. The samples were then centrifuged at 10000$g$ for 5 min, and heme absorbance in the supernatant was measured at 410 nm. Baseline was defined by RBC incubated with PBS only and lysis was normalized to 15 $\mu$M melittin and with osmotic lysis with distilled water. Each measurement represents the average of 3−5 separate experiments $\pm$ SEM. B: Cytotoxicity activity of peptides incubated with MV4:11 cells in suspension and with adherent HEK293T cells in culture. Cytotoxicity was measured using the indicator MTT which quantitates mitochondiral activity. A sample with cells + media was used to determine maximum MTT signal. Media with no cells was used to measure background signal. Treatment of cells with 0.1% TWEEN detergent reduced MTT activity to zero. Cells were treated with peptides in growth media, and then were allowed to recover. The data are the fractional MTT activity in the culture after incubation at 37 °C for 72 h.

of 0.1 $\mu$m and an internal volume of about $1.2 \times 10^{-19}$ L. For a small molecule such as ANTS, present at 10 mM, only around 750 molecules are inside each vesicle. We have previously performed numerical simulations which show that a single water-filled, transmembrane channel of 10 Å diameter leads to complete leakage of a vesicle's contents in only 10 ms (*6*), and requires as few as 6−8 peptides (*48*), equaling a P:L ratio of ~1:10000. This is consistent with the observation that a single protein ion channel can conduct more than $10^6$ ions per second (*51*). Instead, what we observe

here is that, at 1000 peptides per vesicle, only partial leakage of the vesicle contents, typically just a few hundred indicator molecules, occurs with a half-time of several minutes. It is unlikely that these peptides are forming water-filled pores because they would have to have a cumulative lifetime far less than 10 ms. Instead, it is much more likely that the membrane-spanning structure formed by these peptides is not a water-filled channel or pore, but instead is a local non-bilayer, peptide−lipid structure, perhaps a reverse-micelle-like structure, through which a few solute molecules can pass while it exists.

The so-called "carpet model" or "sinking raft" model (*24*) offers the best possible explanation for the formation of such a peptide−lipid "pore" structure and explains our observations in this system. In this model, peptides bind to the membrane surface and self-assemble into peptide-rich domains. The asymmetric transbilayer distribution of peptide causes an imbalance in packing, surface tension, and charge. This imbalance across the membrane drives the formation of transient, non-bilayer, peptide−lipid domains that allow for the transbilayer equilibration, or flip-flop (*52*), of peptides. The translocation of peptides across the bilayer relieves the imbalance and thus leakage stops when the peptides have equilibrated across the bilayer. In this model, leakage occurs concomitantly with peptide translocation, and there is no requirement for a water-filled, transmembrane structure to be present at any time. This type of structure, shown schematically in Figure 10, is consistent with the observation of partial graded leakage of a few hundred indicator molecules from a vesicle to which there are a few hundred peptides bound.

The mechanism of membrane leakage according to the carpet model relies on self-assembled peptide-rich domains, destabilization of the bilayer structure, and formation of non-bilayer structures. In buffer alone the peptides chosen for the study here, which were the most potent 0.1% of the library, are soluble and favor a $\beta$-sheet structure. Because tryptophan fluorescence in buffer (Figure 2; Table 2) indicates water exposure of the tryptophan residue, the solution structure must be composed of small aggregates, or possibly intramolecular $\beta$-sheets. The two studied peptides that are negative for pore formation were found to be random coils in buffer (Figure 4) and at least partially helical in membranes.

Peptide interactions with membranes were characterized by fluorescence spectroscopy, which indicated that these peptides reside predominantly in a configuration where self-assembled $\beta$-strands are at the bilayer interface, exposed to water and probably roughly parallel with the bilayer surface. A small amount of membrane-spanning secondary structure cannot be ruled out. However because leakage stops after about 15 min in vesicles, it is unlikely that there are any equilibrium transmembrane pores.

Addition of these pore-forming peptides to vesicles results in a rapid burst of graded leakage that slows with a half-time of approximately 2−3 min (Figures 5 and 6). Subsequent additions of peptide caused additional bursts of leakage (not shown). For leakage to occur there must be a destabilization of the bilayer. The membrane fusion we observed with the pore-forming peptides, Figure 7, shows that these peptides destabilize the bilayers by disruption of the hydration layer and exposing hydrophobic moieties. Importantly,
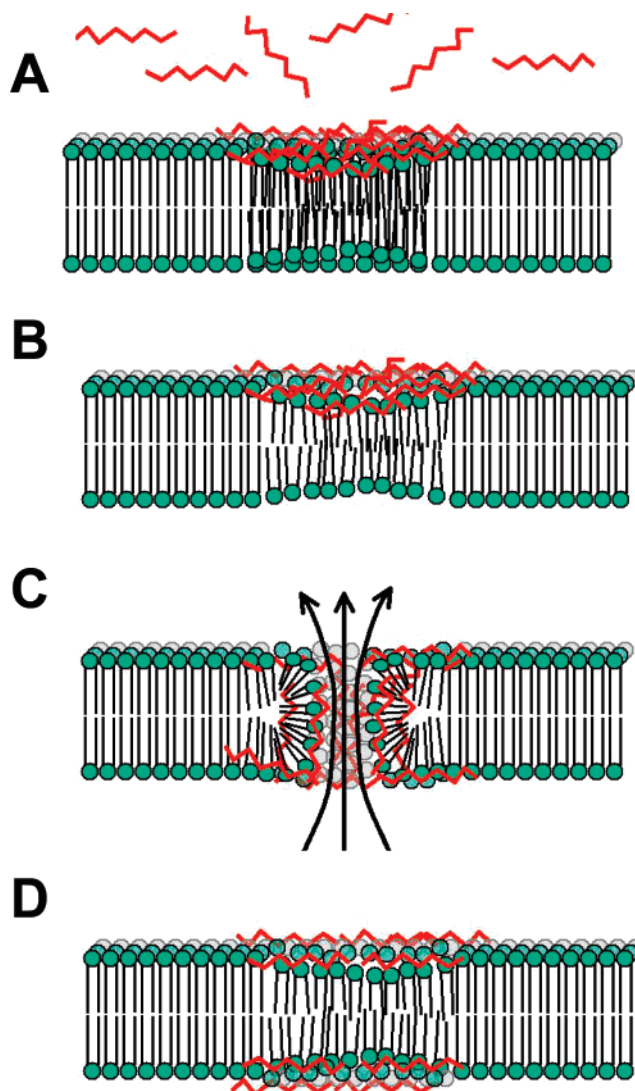


FIGURE 10: The "carpet model" or "sinking raft" model of peptide induced pore formation in lipid vesicles. This model for peptide pore formation explains the observed mechanism of action of many pore-forming, antimicrobial peptides such as the ones we have studied here. In this model peptides bind to a membrane surface A, driven by a combination of hydrophobic and electrostatic interactions, followed by self-assembly into peptide-rich domains, B, driven by the propensity of these peptides to self-assemble into $\beta$-sheets in membranes. The peptide-rich domains are hypothesized to destabilization of the bilayer because of the asymmetry in mass, charge, or surface tension. Relief of the asymmetry occurs when the membrane breaks down, C, and peptide and lipid can undergo transbilayer equilibration. During this transient breakdown of the bilayer integrity, entrapped molecules are also released. In the post-pore structure, D, the peptide is present on both sides of the membrane, therefore there is no asymmetry-driven destabilization and these bilayers do not release their contents.

we showed that fusion itself is not the process that causes leakage, because fusion only occurs at the highest P:L ratios we studied whereas leakage occurs at much lower P:L ratios. These observations are entirely consistent with the carpet model's requirement for self-assembly, destabilization of the bilayer, and formation of non-bilayer structures.

*Activity against Biological Membranes.* The pore-forming peptides discovered by screening the $\beta$-hairpin library in lipid vesicles share features in common with endogenous pore-forming AMP; they are cationic peptides with amphipathic secondary structure and a propensity to self-assemble on

membranes. We hypothesized that the mechanism of pore formation in biological membranes is similar. Therefore, we initiated the studies described here to characterize the antimicrobial, hemolytic, and cytotoxic activity of four similar peptides originating from this framework that have very different structures and functions in vesicles. The potent pore-formers FSKRGY and YGKRGF correspond to the conserved pore-forming sequence motif and display β-sheet content in solution and in membranes (*7*). The selected non-pore-former, AGGKGF, shares the 20 residue framework sequence and some aspects of the pore-forming motif, but was found to be α-helical in membranes and did not cause substantial leakage from vesicles (*7*). The fourth peptide, with the residues GGEDGA in the six varied sites, was designed as a negative control for this work. With acidic instead of basic residues and glycine and alanine in place of the interfacial aromatics, it is as different as possible from the pore-forming motif, while still maintaining the β-hairpin template used in the library. This peptide is largely unstructured when bound to vesicles and is not a potent pore-former in vesicles where it has a small amount of α-helix. The four peptides share 77% sequence identity in their 20-residue framework sequence.

All four peptides YGKRGF, FSKRGY, AGGKGF, and GGEDGA, despite having different activities and different secondary structure in the vesicle experiments, have similarly potent sterilizing antimicrobial activity against the Gram-negative bacteria *Escherichia coli* and *Pseudomonas aeruginosa*. Thus the framework sequence alone, which was not sufficient for pore-forming activity in the more stringent vesicle system and which does not promote a unique secondary structure in vesicles, is apparently sufficient for at least some biological activity. Activity against other classes of microorganisms apparently requires more stringent properties. Only peptides with at least one aspect of the pore-forming motif, YGKRGF, FSKRGY, and AGGKGF, have activity against the Gram-positive bacterium *Staphylococcus aureus* and the fungus *Cryptococcus neoformans*, while the designed negative peptide, GGEDGA, does not have measurable activity against these organisms (Figure 8A).

We show in Figure 8B that the broad spectrum peptides YGKRGF, FSKRGY, and AGGKGF rapidly and completely permeabilize *E. coli* membranes, further supporting the idea that they are acting in a manner that is similar to the natural pore-forming antimicrobial peptides. Interestingly, the designed negative peptide GGEDGA has a much lower propensity to permeabilize microbial membranes. Although GGEDGA is still antimicrobial at this concentration, this result suggests an addition correlation between the vesicle results and the antimicrobial activity. Taken together the experiments on antimicrobial activity suggest a close, but not perfect, correlation between peptide pore formation in vesicle membranes and in biological membranes.

Like many natural antimicrobial peptides, the four peptides tested generally have low activity against mammalian cell membranes at sterilizing antimicrobial concentrations, including sheep and human erythrocytes, and two human cell lines. Interestingly, the peptide AGGKGF, which is negative for pore formation in vesicles and is helical rather than β-sheet, has the highest activity against mammalian cell membranes, lysing human erythrocytes and killing MV4:11 cells at 15 μM. This peptide does not have measurable

**Table 5: Correlation of Structure−Function Relationships**

| peptide | pore formation in vesicles[a] | antimicrobial activity against *E. coli*[b] | broad-spectrum antimicrobial activity[c] | hemolytic or cytotoxic activity[d] |
|---|---|---|---|---|
| indolicidin[e] | yes | yes | yes | no |
| FSKRGY | yes | yes | yes | no |
| YGKRGF | yes | yes | yes | no |
| AGGKGF | no | yes | yes | yes |
| GGEDGA | no | yes | no | no |

[a] Does the peptide cause measurable (>5%) leakage of contents from vesicles made from POPC alone or POPC with 10% POPG or POPC with 10% POPG and 30% cholesterol? [b] Does the peptide have sterilizing antimicrobial activity against *E. coli* at 5 μM or lower concentration? [c] Does the peptide have sterilizing antimicrobial activity against all four organisms studied, *E. coli*, *P. aeruginosa*, *S. aureus*, and *C. neoformans*, at concentrations below 5 μM? [d] Does the peptide cause greater than 50% hemolysis or cytotoxicity for any mammalian cell type at any concentration studied? [e] Indolicidin is a natural pore-forming antimicrobial peptide found in bovine neutrophils.

activity against sheep erythrocytes or the adherent HEK293T cells.

Table 5 shows a summary of the activity of these peptides against vesicles, microbes, and human cell membranes. Peptides with the motif selected in the high-throughput screen, which are pore-forming β-sheets in vesicles (YGKRGF, FSKRGY), have activity against Gram-negative bacteria that is indistinguishable from peptides that are non-pore-forming α-helices (AGGKGF) or mostly random coils (GGEDGA) under the same conditions. However, against a screen of multiple classes of microorganisms, only peptides with at least one aspect of the pore-forming motif have potent antimicrobial activity. AGGKGF, the only peptide studied that has strong activity against mammalian cells, is also a potent antimicrobial peptide, but is helical and does not form pores in vesicles. These results suggest that there is a correlation between pore formation in vesicles and microbial membranes, but that the correlation is imperfect.

*Correlation between Structure and Function in Membranes.* The carpet or sinking raft model is the most commonly accepted model for antimicrobial peptide activity in vesicles (*7, 23, 24, 53*). In this model, peptides self-assemble into peptide-rich domains likened to "rafts" in the outer leaflet of the membrane, which results in a local increase in surface area, surface tension, or electrostatic potential of the outer leaflet relative to inner leaflet, causing strain within the bilayer. The strain is relieved by a structural transition in which transient, membrane-spanning peptide−lipid pore structures form. Peptides and lipids are expected to rapidly equilibrate across the bilayer through these non-bilayer structures. We hypothesize that this model also may explain why the underlying mechanism of action of these types of peptides in biological membranes is not specific to secondary structure or membrane-spanning structures observed in vesicles. Instead, the carpet model, if it is applicable to microbial membranes, would suggest that antimicrobial activity relies on the balance of fundamental peptide−lipid and peptide−peptide interactions that can be mimicked, but not precisely recreated, in model system such as vesicles.

There is ample evidence in the literature supporting the idea that specific structures are not required for antimicrobial activity. Foremost among the lines of evidence is the

remarkable diversity in the sequence, structure, length, and composition of naturally occurring antimicrobial peptides. Furthermore, systematic engineering of several antimicrobial peptides have given fully active analogues that are very different from the parent peptide (*54*). The disulfide-cross-linked, antimicrobial *β*-hairpin peptide lactoferricin retains its antimicrobial biological activity even after 19 of its 25 residues, including all of the disulfide cross-links, are removed, requiring only a core linear hexapeptide that is as active as the 25-residue disulfide-cross-linked parent *β*-hairpin (*55*). In fact many derivatives of lactoferricin are highly active antimicrobial peptides (*56*–*58*). Disulfide-cross-linked variants of our FSKRGY have antimicrobial activity that is indistinguishable from the non-cross-linked peptide (J.R.M. and W.C.W., unpublished observations). As further evidence of the unimportance of specific tertiary structure, it has been shown that reduction of disulfide cross-links in natural AMPs does not always reduce antimicrobial activity (*57*, *59*). Blazyk and colleagues synthesized a series of peptides with different patterns of hydrophobic and hydrophilic residues and tested their antimicrobial activity and secondary structure (*60*). Although biological activity was correlated to amino acid composition, they found a lack of correlation between secondary structure in vesicles and antimicrobial activity. Similarly, Shai and colleagues have studied diastereomeric isomers of pore-forming peptides (e.g. melittin) and found that they do not lose antimicrobial activity when their native secondary structure is abolished by the introduction of multiple D amino acids (*23*, *61*–*63*). On the contrary, such peptides are often better antimicrobial peptides with reduced cytotoxic and hemolytic activity. Similarly Shai and colleagues have shown that large changes in sequence and structure sometimes have little effect on antimicrobial activity (*18*, *23*, *64*, *65*). Based on our findings and on the literature discussed above, we hypothesize that the carpet model, which is clearly consistent with the observed mechanism of pore-forming peptides in vesicles, is also applicable to the mechanism of action of these types of peptides in the membranes of living microbes.

## SUMMARY

In this work, we have used combinatorial chemistry and high-throughput screening as learning tools to study the structure, function, and self-assembly of *β*-sheet, pore-forming peptides in lipid bilayer vesicles and in biological membranes. In vesicle membranes, the mechanism of action of the most potent pore-formers selected from a 26-residue, 9,604 member rational combinatorial library is consistent with the formation of transient peptide–lipid pore domains by the "carpet" or "sinking raft" model in which peptides bind to and self-assemble on the membrane surface, thus driving a transient, non-bilayer peptide–lipid structure that allows polar molecules to leak across membranes. We found no evidence of equilibrium membrane-spanning, water-filled pore structures. The mechanism of action in vesicles suggests a mechanistic connection between the selected pore-formers and natural pore-forming antimicrobial peptides. The data presented here support this idea, although the structure–function relationships that were apparent in the vesicle systems did not always correlate completely with the antimicrobial activity of the same peptides in biological membranes. For example, some peptides with no pore-forming activity in vesicles do have antimicrobial activity. However, because the peptides that are pore-formers in vesicles also have broad-spectrum antimicrobial activity and have little or no cytotoxicity activity, we hypothesize that combinatorial chemistry and vesicle-based high-throughput screens are selecting for peptides with physical properties that are shared by both processes. Results we have obtained recently by screening other libraries strongly support this conclusion (R.R. and W.C.W., unpublished results). In this small sample, the pore-forming peptides selected in the vesicle screen are the ones that are most similar to natural pore-forming antibiotic peptides: they form pores in vesicles by a carpet model mechanism, they have broad-spectrum antimicrobial activity, and they have little hemolytic or cytotoxicity activity.

## REFERENCES

1. Ramachandran, R., Heuck, A. P., Tweten, R. K., and Johnson, A. E. (2002) Structural insights into the membrane-anchoring mechanism of a cholesterol-dependent cytolysin, *Nat. Struct. Biol. 9*, 823–827.
2. Gouaux, E. (1998) α-Hemolysin from *Staphylococcus aureus*: An archetype of *β*-barrel, channel-forming toxins, *J. Struct. Biol. 121*, 110–122.
3. Lacy, D. B., and Collier, R. J. (2002) Structure and function of anthrax toxin, *Curr. Top. Microbiol. Immunol. 271*, 61–85.
4. Zasloff, M. (2002) Antimicrobial peptides of multicellular organisms, *Nature (London) 415*, 389–395.
5. Yount, N. Y., and Yeaman, M. R. (2004) Multidimensional signatures in antimicrobial peptides, *Proc. Natl. Acad. Sci. U.S.A. 101*, 7363–7368.
6. Wimley, W. C., Selsted, M. E., and White, S. H. (1994) Interactions between human defensins and lipid bilayers: Evidence for the formation of multimeric pores, *Protein Sci. 3*, 1362–1373.
7. Rausch, J. M., Marks, J. R., and Wimley, W. C. (2005) Rational combinatorial design of pore-forming *β*-sheet peptides, *Proc. Natl. Acad. Sci. U.S.A. 102*, 10511–10515.
8. Wimley, W. C., and White, S. H. (2004) Reversible unfolding of *β*-sheets in membranes: a calorimetric study, *J. Mol. Biol. 342* (3), 703–711.
9. Rausch, J. M., and Wimley, W. C. (2001) A high-throughput screen for identifying transmembrane pore-forming peptides, *Anal. Biochem. 293*, 258–263.
10. Wimley, W. C. (2003) The versatile *β*-barrel membrane protein, *Curr. Opin. Struct. Biol. 13*, 404–411.
11. Wimley, W. C. (2002) Toward genomic identification of *β*-barrel membrane proteins: composition and architecture of known structures, *Protein Sci. 11*, 301–312.
12. Schulz, G. E. (2002) The structure of bacterial outer membrane proteins, *Biochim. Biophys. Acta 1565*, 308–317.
13. Wimley, W. C., and White, S. H. (1996) Experimentally determined hydrophobicity scale for proteins at membrane interfaces, *Nat. Struct. Biol. 3*, 842–848.
14. Ladokhin, A. S., Selsted, M. E., and White, S. H. (1997) Bilayer interactions of indolicidin, a small antimicrobial peptide rich in tryptophan, proline, and basic amino acids, *Biophys. J. 72*, 794–805.
15. White, S. H., Wimley, W. C., and Selsted, M. E. (1995) Structure, function, and membrane integration of defensins, *Curr. Opinion Struct. Biol. 5*, 521–527.

16. Yeaman, M. R., and Yount, N. Y. (2003) Mechanisms of antimicrobial peptide action and resistance, *Pharmacol. Rev. 55*, 27−55.

17. White, S. H., and Wimley, W. C. (1999) Membrane protein folding and stability: physical principles, *Annu. Rev. Biophys. Biomol. Struct. 28*, 319−365.

18. Papo, N., and Shai, Y. (2003) Can we predict biological activity of antimicrobial peptides from their interactions with model phospholipid membranes?, *Peptides 24*, 1693−1703.

19. (2006) Antimicrobial Peptides Database. http://aps.unmc.edu/AP/main.html.

20. Zhang, L., and Falla, T. J. (2004) Cationic antimicrobial peptides— an update, *Expert. Opin. Invest. Drugs 13*, 97−106.

21. Huang, H. W., Chen, F. Y., and Lee, M. T. (2004) Molecular mechanism of peptide-induced pores in membranes, *Phys. Rev. Lett. 92*, 198304.

22. Wallace, B. A. (1998) Recent advances in the high resolution structures of bacterial channels: Gramicidin A, *J. Struct. Biol. 121*, 123−141.

23. Shai, Y., and Oren, Z. (2001) From "carpet" mechanism to de-novo designed diastereomeric cell-selective antimicrobial peptides, *Peptides 22*, 1629−1641.

24. Pokorny, A., and Almeida, P. F. (2004) Kinetics of dye efflux and lipid flip-flop induced by delta-lysin in phosphatidylcholine vesicles and the mechanism of graded release by amphipathic, α-helical peptides, *Biochemistry 43*, 8846−8857.

25. Brahmachary, M., Krishnan, S. P., Koh, J. L., Khan, A. M., Seah, S. H., Tan, T. W., Brusic, V., and Bajic, V. B. (2004) ANTI-MIC: a database of antimicrobial sequences, *Nucleic Acids Res. 32*, D586−D589.

26. Wang, Z. and Wang, G. (2004) APD: the Antimicrobial Peptide Database, *Nucleic Acids Res. 32*, D590−D592.

27. Bulet, P., Stocklin, R., and Menin, L. (2004) Anti-microbial peptides: from invertebrates to vertebrates, *Immunol. Rev. 198*, 169−184.

28. Silvestro, L., Weiser, J. N., and Axelsen, P. H. (2000) Antibacterial and antimembrane activities of cecropin A in Escherichia coli, *Antimicrob. Agents Chemother. 44*, 602−607.

29. Grant, G. A. (1992) *Synthetic Peptides:A User's Guide*, WH Freeman and Company, New York.

30. Atherton, E. and Sheppard, R. C. (1989) *Solid phase peptide synthesis* IRL Press, Oxford.

31. Hope, M. J., Bally, M. B., Mayer, L. D., Janoff, A. S., and Cullis, P. R. (1986) Generation of multilamellar and unilamellar phospholipid vesicles, *Chem. Phys. Lipids 40*, 89−109.

32. Mayer, L. D., Hope, M. J., and Cullis, P. R. (1986) Vesicles of variable sizes produced by a rapid extrusion procedure, *Biochim. Biophys. Acta 858*, 161−168.

33. Ladokhin, A. S., Wimley, W. C., Hristova, K., and White, S. H. (1997) Mechanism of leakage of contents of membrane vesicles determined by fluorescence requenching, *Methods Enzymol. 278*, 474−486.

34. Ladokhin, A. S., Wimley, W. C., and White, S. H. (1995) Leakage of membrane vesicle contents: Determination of mechanism using fluorescence requenching, *Biophys. J. 69*, 1964−1971.

35. White, S. H., Wimley, W. C., Ladokhin, A. S., and Hristova, K. (1998) Protein folding in membranes: Determining the energetics of peptide-bilayer interactions, *Methods Enzymol. 295*, 62−87.

36. Ladokhin, A. S., Jayasinghe, S., and White, S. H. (2000) How to measure and analyze tryptophan fluorescence in membranes properly, and why bother?, *Anal. Biochem. 285*, 235−245.

37. Montich, G., Scarlata, S., McLaughlin, S., Lehrmann, R., and Seelig, J. (1993) Thermodynamic characterization of the association of small basic peptides with membranes containing acidic lipids, *Biochim. Biophys. Acta 1146*, 17−24.

38. Murray, D., Hermida-Matsumoto, L., Buser, C. A., Tsang, J., Sigal, C. T., Ben-Tal, N., Honig, B., Resh, M. D., and McLaughlin, S. (1998) Electrostatics and the membrane association of Src: Theory and experiment, *Biochemistry 37*, 2145−2159.

39. Struck, D. K., Hoekstra, D., and Pagano, R. E. (1981) Use of resonance energy transfer to monitor membrane fusion, *Biochemistry 20*, 4093−4099.

40. Belokoneva, O. S., Villegas, E., Corzo, G., Dai, L., and Nakajima, T. (2003) The hemolytic activity of six arachnid cationic peptides is affected by the phosphatidylcholine-to-sphingomyelin ratio in lipid bilayers, *Biochim. Biophys. Acta 1617*, 22−30.

41. Ben-Tal, N., Honig, B., Miller, C., and McLaughlin, S. (1997) Electrostatic binding of proteins to membranes. Theoretical predictions and experimental results with charybdotoxin and phospholipid vesicles, *Biophys. J. 73*, 1717−1727.

42. Wimley, W. C., and White, S. H. (2000) Determining the membrane topology of peptides by fluorescence quenching, *Biochemistry 39*, 161−170.

43. Manning, M. C., Illangasekare, M., and Woody, R. W. (1988) Circular dichroism studies of distorted α-helices, twisted β-sheets, and β-turns, *Biophys. Chem.* 77−86.

44. Wimley, W. C., Hristova, K., Ladokhin, A. S., Silvestro, L., Axelsen, P. H., and White, S. H. (1998) Folding of β-sheet membrane proteins: A hydrophobic hexapeptide model, *J. Mol. Biol. 277*, 1091−1110.

45. Hristova, K., Selsted, M. E., and White, S. H. (1996) Interactions of monomeric rabbit neutrophil defensins with bilayers: Comparison with dimeric human defensin HNP-2, *Biochemistry 35*, 11888−11894.

46. Bohrer, M. P., Deen, W. M., Robertson, C. R., Troy, J. L., and Brenner, B. M. (1979) Influence of molecular configuration on the passage of macromolecules across glomerular capillary wall, *J. Gen. Physiol. 74*, 583−593.

47. Sanny, C. G., and Price, J. A. (1999) Analysis of nonlinear quenching of terbium(III):dipicolinic acid complex fluorescence by chelators and chelate-conjugated macromolecules, *Bioconjugate Chem. 10*, 141−145.

48. Parente, R. A., Nir, S., and Szoka, F. (1990) Mechanism of leakage of phospholipid vesicle contents induced by the peptide GALA, *Biochemistry 29*, 8720−8728.

49. Shepard, L. A., Heuck, A. P., Hamman, B. D., Rossjohn, J., Parker, M. W., Ryan, K. R., Johnson, A. E., and Tweten, R. K. (1998) Identification of a membrane-spanning domain of the thiol-activated pore-forming toxin Clostridium perfringens perfringolysin O: an α-helical to β-sheet transition identified by fluorescence spectroscopy, *Biochemistry 37*, 14563−14574.

50. Selsted, M. E., Novotny, M. J., Morris, W. L., Tang, Y.-Q., Smith, W., and Cullor, J. S. (1992) Indolicidin, a novel bactericidal tridecapeptide amide from neutrophils, *J. Biol. Chem. 267*, 4292−4295.

51. Hille, B. (1972) The permeability of the sodium channel to metal cations in myelinated nerve, *J. Gen. Physiol. 59*, 637−658.

52. Fattal, E., Nir, S., Parente, R. A., and Szoka, F. C. (1994) Pore-forming peptides induce rapid phospholipid flip-flop in membranes, *Biochemistry 33*, 6721−6731.

53. Rausch, J. M. (2004) Design and characterization of pore-forming peptides from a combinatorial library, Ph.D. Dissertation, Tulane University Health Sciences Center, New Orleans, LA.

54. Won, H. S., Jung, S. J., Kim, H. E., Seo, M. D., and Lee, B. J. (2004) Systematic peptide engineering and structural characterization to search for the shortest antimicrobial peptide analogue of gaegurin 5, *J. Biol. Chem. 279*, 14784−14791.

55. Schibli, D. J., Hwang, P. M., and Vogel, H. J. (1999) The structure of the antimicrobial active center of lactoferricin B bound to sodium dodecyl sulfate micelles, *FEBS Lett. 446*, 213−217.

56. Nguyen, L. T., Schibli, D. J., and Vogel, H. J. (2005) Structural studies and model membrane interactions of two peptides derived from bovine lactoferricin, *J. Pept. Sci. 11*, 379−389.

57. Vogel, H. J., Schibli, D. J., Jing, W., Lohmeier-Vogel, E. M., Epand, R. F., and Epand, R. M. (2002) Towards a structure-function analysis of bovine lactoferricin and related tryptophan- and arginine-containing peptides, *Biochem. Cell Biol. 80*, 49−63.

58. Ulvatne, H., Haukland, H. H., Olsvik, O., and Vorland, L. H. (2001) Lactoferricin B causes depolarization of the cytoplasmic membrane of Escherichia coli ATCC 25922 and fusion of negatively charged liposomes, *FEBS Lett. 492*, 62−65.

59. Hunter, H. N., Jing, W., Schibli, D. J., Trinh, T., Park, I. Y., Kim, S. C., and Vogel, H. J. (2005) The interactions of antimicrobial peptides derived from lysozyme with model membrane systems, *Biochim. Biophys. Acta 1668*, 175−189.

60. Jin, Y., Hammer, J., Pate, M., Zhang, Y., Zhu, F., Zmuda, E., and Blazyk, J. (2005) Antimicrobial activities and structures of two linear cationic peptide families with various amphipathic β-sheet and α-helical potentials, *Antimicrob. Agents Chemother. 49*, 4957−4964.

61. Papo, N., and Shai, Y. (2003) New lytic peptides based on the D,L-amphipathic helix motif preferentially kill tumor cells compared to normal cells, *Biochemistry 42*, 9346−9354.

62. Avrahami, D., and Shai, Y. (2002) Conjugation of a magainin analogue with lipophilic acids controls hydrophobicity, solution assembly, and cell selectivity, *Biochemistry 41*, 2254−2263.

63. Oren, Z., Hong, J., and Shai, Y. (1999) A comparative study on the structure and function of a cytolytic α- helical peptide and its antimicrobial β-sheet diastereomer, *Eur. J. Biochem. 259*, 360−369.

64. Papo, N., and Shai, Y. (2004) Effect of drastic sequence alteration and D-amino acid incorporation on the membrane binding behavior of lytic peptides, *Biochemistry 43*, 6393−6403.

65. Oren, Z., and Shai, Y. (1996) A class of highly potent antibacterial peptides derived from pardaxin, a pore-forming peptide isolated from Moses sole fish *Pardachirus marmoratus*, *Eur. J. Biochem. 237*, 303−310.